# A model of diffuse attenuation of downwelling irradiance for ecosystem models

Bouchra Nechad[a], Kevin Ruddick[a]
[a]Management Unit of the North Sea Mathematical Models (MUMM), Royal Belgian Institute for Natural Science (RBINS), 100, Gulledelle, Brussels, 1200, Belgium
Email: B.Nechad@mumm.ac.be

## ABSTRACT

Estimation of the underwater attenuation of light is important to ecosystem modellers, who require information on Photosynthetically Available Radiation ( $PAR$ ), and on the euphotic depth for calculation of primary production. Characterisation of these processes can be achieved by determining the diffuse attenuation coefficient of $PAR$ , $KPAR$ . A review of bio-optical models of the spectral diffuse attenuation coefficient for downwelling irradiance, $K_d$ , is presented and stresses the necessity for a better knowledge and parameterization of these coefficients.

In the second part of this work, radiative transfer simulations were carried out to model $K_{dZ1\%}$ the spectral diffuse attenuation of downwelling irradiance averaged over the euphotic depth $Z_{1\%}$ (depth where the downwelling irradiance is 1% of its surface value). This model takes into account the effects of varying sun zenith angle and cloud cover and needs absorption and backscattering coefficients (the inherent optical properties, IOPs) as input. It provides average and maximum relative errors of 1% and 5% respectively, for sun zenith angles [0°-50°] and of 1.7% and 12% respectively at higher sun zenith angles. A relationship was established between $K_{dZ1\%}$ at a single wavelength (590nm) and $KPAR$ at $Z_{PAR1\%}$ (where $PAR$ is 1% of its value at the surface) which allows for a direct expression of $KPAR_{ZPAR1\%}$ in terms of inherent optical properties, sun angle and cloudiness. This model provides estimates of $KPAR$ within 25% (respectively 40%) relative errors respectively with a mean relative error less than 7% (respectively 9%) for sun zenith angles ranging from 0° to 50° (respectively higher than 50°). A similar method is applied to derive a model for the diffuse attenuation of photosynthetically usable radiation, $KPUR_{ZPUR1\%}$ , with similar performance.

**Keywords:** diffuse attenuation coefficient of downwelling irradiance, average cosine, photosynthetically available radiation, photosynthetically usable radiation, semi-analytical model, ecosystem models

## 1. INTRODUCTION

Since the early 1950s, eutrophication in lakes and coastal waters has become a phenomenon of concern for water quality managers and society in general [1]. The community of limnologists was the first to undertake research establishing the eutrophication status in lakes and modeling the response of these waters to changes in nutrient inputs [2]. [2] presents a review of such models that estimate the primary production from the hydraulic and morphometric fields and nutrient loads. However, these models show diverging responses to a given nutrient loading on a seasonal scale [3], because they lack information on the optical conditions as pointed out by [4]. A review by [5] on light attenuation parameterization in the ecological models published from 1976 to 2003, shows that these models are generally based on a formulation of the diffuse attenuation coefficient of the photosynthetically available radiation, $KPAR$ , or of the downwelling irradiance, $K_d$ (it was reported that this parameter was sometimes ambiguously defined) as function of CHL, and underestimate $KPAR$ in shallow waters. In a number of estuarine and coastal zones, it has been shown that $K_d$ is almost entirely governed by suspended particulate matter ( $SPM$ ) [6-8]. In others, coloured dissolved organic matter ( $CDOM$ ) [5] may also be important in determining $KPAR$ . In particular, the timing of algal blooms may be extremely sensitive to the light available underwater [9]. A significant improvement in the prediction of algal bloom amplitudes and timing was obtained by integration of suspended matter loads in the modeling of $KPAR$ in coastal waters [10, 11].

Remote Sensing of the Coastal Ocean, Land, and Atmosphere Environment, edited by Robert J. Frouin, Hong Rhyong Yoo, Joong-Sun Won, Aiping Feng, Proc. of SPIE Vol. 7858, 78580D · © 2010 SPIE · CCC code: 0277-786X/10/$18 · doi: 10.1117/12.872979

## 2. $K_D$ ALGORITHMS

The light available for photosynthesis, $PAR$ may be determined from the (omnidirectional) scalar irradiance, $E_o$ using [12] [13] in either energetic Eq(1.a) or quantum units Eq(1.b):

$$\text{a. } PAR = \int_{400nm}^{700nm} E_o(\lambda)\, d\lambda \ [Wm^{-2}] \qquad \text{b. } PAR = \frac{1}{hc}\int_{400nm}^{700nm} \lambda E_o(\lambda)\, d\lambda \ [photons\, m^{-2} s^{-1}] \tag{1}$$

Following this definition, the diffuse attenuation coefficient for scalar irradiance, $K_o$, might be of more direct importance in the estimation of the attenuation coefficients of $PAR$, $KPAR$. However, in the present review the diffuse attenuation coefficient for downwelling irradiance, $K_d$ defined by:

$$K_d(z,\lambda) = -\frac{dE_d(z,\lambda)}{E_d(z,\lambda)\, dz} \tag{2}$$

is considered, because the values of $K_d$ and $K_o$ are generally quite similar [12, 14] and most studies consider $K_d$ since it is more easily measured. $K_d$ is an apparent optical property (AOP) which may be computed from water IOPs and the angular dependence of the surface light field (and also the spectral dependence if $KPAR$ is required). Because of the lack of information on these IOPs, the first algorithms set up for remote sensing retrieval of $K_d$ were empirical and designed as part of the inverse problem, thus giving $K_d$ as a function of the blue-to-green ratio of water-leaving radiance or remote sensing reflectance [15-18]:

$$K_d(490) = f\left(\frac{L_{blue}}{L_{green}}\right) \tag{3}$$

This is described as the direct *one-step* scheme (see Figure 1 in [19]). This formulation is most appropriate for "Case 1" waters where optical properties are determined entirely by algal particles and will therefore not perform well in "Case 2" waters with significant non algal particles or $CDOM$ not related to phytoplankton.

Algorithms relating $K_d$ to water constituents have been first developed for the open ocean where strong correlations were found between $CHL$ and $K_d$ [20, 21], $CHL$ being the major component that controls light attenuation in these case 1 waters. Therefore, $K_d$ –algorithms can be designed in a *two-step* scheme:

$$\text{a. } CHL = f\left(\frac{L_{blue}}{L_{green}}\right) \qquad \text{b. } K_d = K_w + \chi\, CHL^{\gamma} \tag{4}$$

where $\chi$ and $\gamma$ are determined empirically and $CHL$ is retrieved as a spectral ratio of water reflectance (e.g. the OC3, OC4 algorithms).

A generalization of Eq(4.b) expresses light attenuation as a linear function of the concentrations of the main optically active components in case 2 waters, $C_i$ (e.g. i being generally $CHL$, $CDOM$, $SPM$). Such equations follow the form [22, 23]:

$$K_d = K_w + \sum_i \chi_i\, C_i^{\ \gamma_i} \tag{5}$$

where $K_w$ is the diffuse attenuation coefficient due to water and $\chi_i, \gamma_i$ are empirically determined from field measurements of light attenuation and concentrations $C_i$. This is also a two-steps method which requires the estimates of $C_i$ from satellite-derived IOPs or from satellite radiances or reflectances $C_i = f(R_{rs})$. Linear, logarithmic or exponential functions of $C_i$ were explored to predict $K_d$ and showed equivalent performance in the study of [8]. It is noted that while linear addition of IOPs, such as components of the total absorption coefficient, are theoretically rigorous, the linear

addition of components of $K_d$ as suggested in (5) is a more empirical approximation which "should work reasonably well near the surface but should lead to systematic errors as depth is increased" [24].

Equations like (5) find their origin in the relationships linking $K_d$ to IOPs [25], which are established analytically, based on the radiative transfer equation (RTE) [26-29]. [30] presented a review of analytical algorithms a.o. [26, 31-33] -some examples are provided in Table 1- and set up a generic model derived from [31] (Eq(9) in Table 1, which is equivalent to Eq(10) by [34]). However, the difficulty in such a "full" model is the need to characterize RTE parameters like the shape factors and the average cosines (see Table 1) which remain poorly documented in turbid waters. An alternative is to use model-generated lookup tables such as the model of [34].

To achieve this, [34] used a semi-analytical method to parameterize the dependency of depth-averaged $K_d$ on water IOPs and on the varying illumination conditions in a clear sky, using numerical simulations of the RTE. They carried out Hydrolight simulations with a large set of artificial IOPs, reformulated the RTE of [29, 31] which led to the expression for the depth-averaged $K_d$, noted hereafter by $\overline{K}_d$:

$$\overline{K}_{d(z,\theta)} = m_{0(z,\theta)}a + m_{1(z,\theta)}\left[1 - m_{2(z,\theta)}e^{-m_{3(z,\theta)}a}\right]b_b \tag{6}$$

where $a$ and $b_b$ are the total absorption and backscattering coefficients. $m_0$, $m_1$, $m_2$, $m_3$ and $\overline{K}_d$ are varying with the depth $z$ and solar zenith angle $\theta$. The $4m$-coefficients were determined via regression analysis and a good approximation was found for $K_d$ integrated from the surface to the depth $Z_{10\%}$ where the downwelling irradiance reaches 10% of its value at the surface (see $\overline{K}_{d(E10\%)}$ given by Eq(11), Table 1).

## 3. METHOD AND DATA

In this paper, an extension of the model (6) to the case of clouded sky is presented, using a similar approach and data sets as in [34]. Here, the RTE is rewritten as in Eq(10), Table 1, then the irradiance reflectance, $R$, is replaced by $fb_b / Qa$ following the reflectance model of [35]:

$$\frac{K_d}{a} = \frac{1}{\mu_d} + \frac{r_d}{\mu_d}\frac{b_b}{a} - \frac{r_u}{\mu_u}\frac{f}{Q}\left(\frac{b_b}{a}\right)^2 \tag{7}$$

Applying the definition of the depth-averaged $\overline{K}_d$ in [34] to the euphotic depth $Z_{x\%}$ where the downwelling irradiance is $x\%$ of its surface value, and considering the average depth parameters $m_0'$, $m_1'$ and $m_2'$ respectively associated to the local depth parameters $1/\mu_d$, $r_d/\mu_d$ and $fr_u/Q\mu_u$, (7) becomes:

$$\frac{\overline{K}_d}{a} = m_0' + m_1'\frac{b_b}{a} - m_2'\left(\frac{b_b}{a}\right)^2 \tag{8}$$

where $m_0'$, $m_1'$ and $m_2'$ vary spectrally, with depth, $Z_{x\%}$, sun zenith angle, $\theta$, and percentage cloudiness, $Cc$, whereas $a$ and $b_b$ vary only with wavelengths and are assumed constant over the depth.

For Hydrolight simulations, the input data are:

- $\theta$ used to determine the direct $E_d^{dir}$ and diffuse $E_d^{dif}$ spectral irradiances incident onto the sea surface, for typical atmospheric conditions using the model of [36]. These irradiances are adapted in Hydrolight to the input $Cc$ using the ratio of global radiation for a given cloud amount to the clear-sky radiation based on the formula of [37], thus the ratio $E_d^{dir}/E_d^{dif}$ varies with cloudiness $Cc > 25\%$ following $E_d^{dir}/E_d^{dif} = \left(1 - Cc^2\right)/\left(0.43 + Cc^2\right)$.

-100 pairs of total absorption and scattering spectral coefficients, picked up (1 out of every 5 pairs, as in [34], but only at 31 wavelengths from 400nm to 700nm) from the set of 500 pairs of artificial IOPs provided by the IOCCG web site

(http://www.ioccg.org/groups/OCAG_data.html)[38]. The average Petzold particle phase function is used here and the backscattering coefficients retrieved from the total scattering coefficients assuming a particle backscatter ratio equal to 0.0183. These IOPs are taken constant along the depth.

Table 1: $K_d$ -IOPs relationships. $G$ is a function of the volume scattering function and $\mu_d$ and $\mu_u$ are respectively the downwelling and upwelling average cosines, $\mu_d^{0-}$ is the downwelling average cosine just below the water surface and $\mu_0$ is the cosine of the sun zenith angle. The factors $r_d$ and $r_u$ respectively refer to the shape factors for downwelling and upwelling scattering [29, 31] . $R$ is the subsurface irradiance reflectance. $K_d$ is the attenuation coefficient at a local depth and $\bar{K}_d$ at an average depth (here, the euphotic zone).

| Reference | Model |
|---|---|
| Gordon et al 1975 [26] | $K_d = \frac{a+b_b}{\mu_0}$ |
| Sathyendranath et al 1989 [32] | $K_d = \frac{a+b_b}{\mu_d}$ |
| Smith and Baker 1981[39] | $K_d = a + b_b$ |
| Aas 1987 [31] | $K_d = \frac{a}{\mu_d}\left[1+\frac{b_b}{a}\right]$, $K_d = \frac{a}{\mu_d}\left[1+r_d\frac{b_b}{a}\right]$ |
| Kirk 1984 [40], Kirk 1991 [33] | $\bar{K}_d = \frac{a}{\mu_d^{0-}}\left[1+G\left(\mu_d^{0-}\right)\frac{b}{a}\right]^{0.5}$ |
| Dekker et al 2001 [30] | $K_d = \frac{a}{\mu_d}\left[1+r_d\frac{b_b}{a}\left(1-\frac{r_u\mu_d}{\mu_u+\mu_d}\frac{b_b}{a+kb_b}\right)\right]$ (9)<br>$k = \frac{r_u\mu_d + r_d\mu_u}{\mu_u+\mu_d}$ |
| Lee et al 2005[34] | $K_d = \frac{1}{\mu_d}a + \left[\frac{r_d}{\mu_d} - \frac{r_u R}{\mu_u}\right]b_b$ (10)<br>$\bar{K}_{d(E10\%)} = \left(1+0.005\theta_0\right)a + 3.47b_b$ (11) |

Simulations were run with 7 different sun zenith angles and 7 values of percentage cloudiness and the results stored for 19 underwater depths and one above the surface for irradiance data (see details in Table 2). From the irradiance profiles, estimates of the photic depths $Z_{x\%}$ where the downwelling irradiance is equal to $x\%\left(x=1,10,50,75,95\right)$ of its surface value were computed, first by identifying the nearest discrete depths where $E_d\left(x\%\right)$ is found, then by a logarithmic interpolation to estimate the exact depth of $E_d\left(x\%\right)$. The corresponding photic depth-averaged attenuation coefficients were retrieved from the $Z_{x\%}$ using: $\bar{K}_d\left(Z_{x\%}\right) = -\log\left(x\%\right)/Z_{x\%}$. For each sun zenith angle and each cloudiness value, about 2500 and 2800 spectral values of $Z_{1\%}$ and $Z_{5\%}$ respectively and 3100 values for $Z_{10\%}$ and $Z_{95\%}$ could be obtained for the 100 pairs of IOPs, when these photic depths were less than 40m (the maximum depth requested in the simulations within HYDROLIGHT). When $Z_{x\%}$ were deeper than 40m, especially for IOPs of very clear waters, they were discarded.

Table 2: The input sun zenith and percentage cloudiness values provided to Hydrolight simulations, the requested output water depths and the computed photic depths.

| **Hydrolight parameters** | **Selected values** |
|---|---|
| Sun zenith angle (°) | 0, 10, 20, 30, 40, 50, 60 |
| Cloudiness (%) | 0, 25, 50, 75, 90, 95, 100 |
| Depths (m) | $0^+$, $0^-$, 0.1, 0.25, 0.5, 1, 1.5, 2, 2.5, 5, 6.5, 8.5, 10, 12.5, 20, 25, 30, 40 |
| Photic depths (%) | 1, 10, 50, 95 |

## 4. CALIBRATION OF KD ALGORITHM

The variations of $\overline{K}_d / a$ with $a$ and $b_b / a$ in the clear sky case have been extensively analysed in [34] for depths 1, 5, 10 and 20m. The $m_0$ coefficient was graphically displayed as the intercept in Eq(6) (Figures 2.a and 3.a of [34]), before being numerically estimated, and the same approach was used to determine the behaviour of the second term in Eq(6). The coefficient $m_0^{'}$ in the new formulation (8) is similar to $m_0$ defined in [34]. Since $m_0^{'}$ is the integration of the path mean inverse cosine, $1/\mu_d$, from the surface of water down to a given photic depth, $m_0^{'}$ will be referred to as the *photic depth mean inverse cosine*. Similarly, $m_1^{'} b_b$ is related to the term $r_d b_b / \mu_d$ which is the diffuse backward scattering function for downwelling irradiance [28, 29], so $m_1^{'}$ is called here the *photic depth diffuse backscatter*.

To compare the present study with that of [34] for the depth-average attenuation coefficient at $Z_{10\%}$ and at sun zenith angle $\theta$=30°, Eq(6) is used with the coefficients listed for $\overline{K}_{d(E10\%)}$ in Table 2 of [34] and Eq(8) is regressed with the Hydrolight-derived $\overline{K}_d / a$ at $Z_{10\%}$ and $b_b / a$ data sets, giving:

$$\frac{\overline{K}_d(Z_{10\%})}{a} = 1.1 + 4.5\frac{b_b}{a} - 3.1\left(\frac{b_b}{a}\right)^2 \qquad (12)$$

Figure 1 plots the resulting $\overline{K}_d(Z_{10\%})$ following equations (6) and (12), for sun at 30° and clear sky conditions. These show that the second term in Eq(6) is not adapted for higher backscattering, for instance in turbid waters, whereas a formulation like Eq(8) with the second order $b_b / a$ is more appropriate.

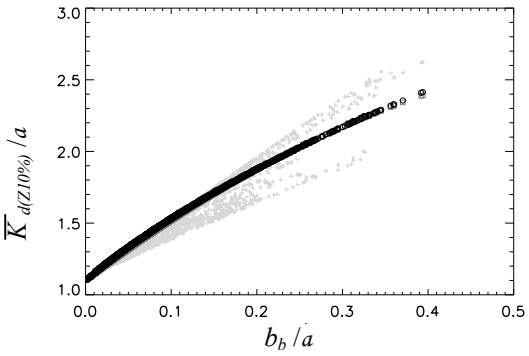


Figure 1: $\overline{K}_d(Z_{10\%})/a$ versus $b_b/a$ for clear sky and sun zenith angle 30° (3100 $\overline{K}_d(Z_{10\%})/a$ data corresponding to the 100 pairs of IOPs taken at 31 wavelengths). $\overline{K}_d(Z_{10\%})/a$ derived from Hydrolight are plotted in black circles, those modeled by Eq(6) are in light grey plus symbols and by Eq(12) in grey squares.

In the present work, non linear regression analysis were applied to Eq(9), using $b_b/a$ data and Hydrolight derived $\overline{K}_d(Z_{1\%})$, $\overline{K}_d(Z_{10\%})$, $\overline{K}_d(Z_{50\%})$ and $\overline{K}_d(Z_{95\%})$, to determine the corresponding coefficients $m_0'$, $m_1'$ and $m_2'$. In the following sections 4.1 to 4.3, the variations of these coefficients with cloudiness and with sun zenith angle are examined globally for the photic depths $Z_{1\%}$, $Z_{5\%}$, $Z_{10\%}$ and $Z_{95\%}$ with a focus on $Z_{1\%}$.

### 4.1 The variations of $m_0'$

The $Z_{1\%}$-photic depth mean cosine forms the intercept in Figure 2 (and in Figure 3), where more than 2450 data of $\overline{K}_d(Z_{1\%})/a$ are plotted against the corresponding $b_b/a$ taken at 31 wavelengths for various cloudiness and zenith angles values. These figures show that the relative variation in $\overline{K}_d/a$ for a given value of $b_b/a$ may reach 10% with a changing cloudiness and 20% for a varying sun zenith angle.

The coefficients $m_0'$ resulting from non linear regression analysis using Eq(9), $b_b/a$ data and Hydrolight derived $\overline{K}_d(Z_{1\%})$, $\overline{K}_d(Z_{10\%})$, $\overline{K}_d(Z_{50\%})$ and $\overline{K}_d(Z_{95\%})$ are plotted in Figure 4 from which the impact of the cloudiness may be summarized as follows:

- for $\theta$ between 0° and 40°, an increase in the cloudiness induces an increase in $m_0'$, with a rate that is higher for lower $\theta$.
- At $\theta$ ranging from 40° to 60°, $m_0'$ decreases with increasing cloudiness.
- At $\theta$=40°, the variations in percentage cloudiness affects only slightly $m_0'$ at photic depths higher than 50% and have almost no effect at deeper photic depths ($Z_{10\%}$, $Z_{1\%}$).

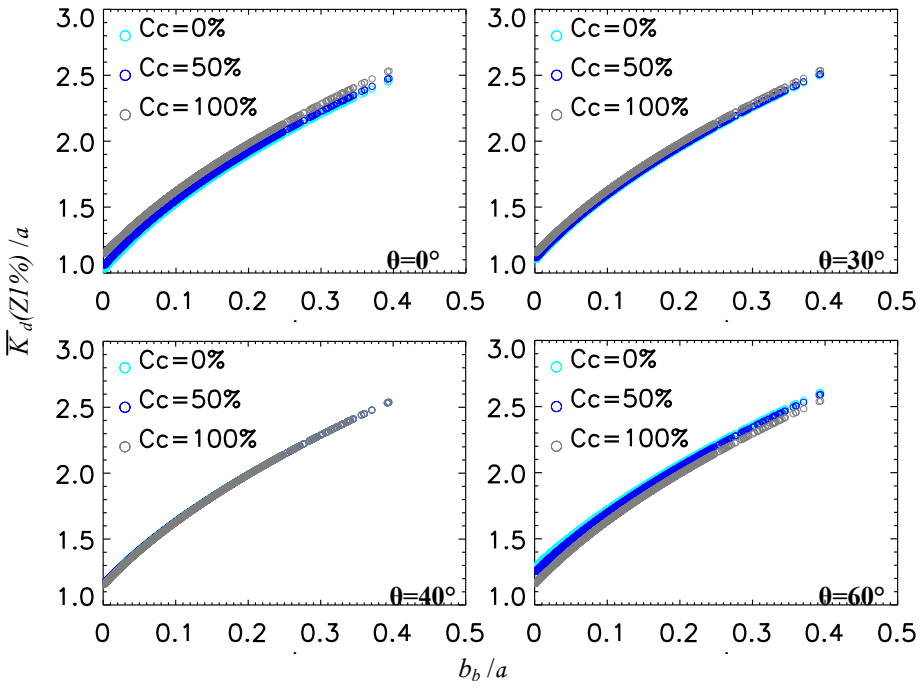


Figure 2: $\overline{K}_d(Z_{1\%})/a$ versus $b_b/a$ for varying cloudiness values (0, 50 and 100%), each graph displays about 2500 $\overline{K}_d(Z_{1\%})/a$ data corresponding to the 100 pairs of IOPs taken at 31 wavelengths and computed for a given sun zenith angle (θ=0, 30, 40 and 60°).

- The difference between the values of $m_0'$ computed for each photic depth and the average value of $m_0'$ over the 4 photic depths $Z_{x\%,x=1,10,50,95}$ (plotted as a dashed black line in Figure 4) remains quite low (less than 4%).

Moreover, the variations of $1/\mu_d^{0+}$ (the path average inverse cosine just above the water surface, not shown here) with $\theta$ and $Cc$ are quite similar to those of the photic depth mean cosine $m_0'$.

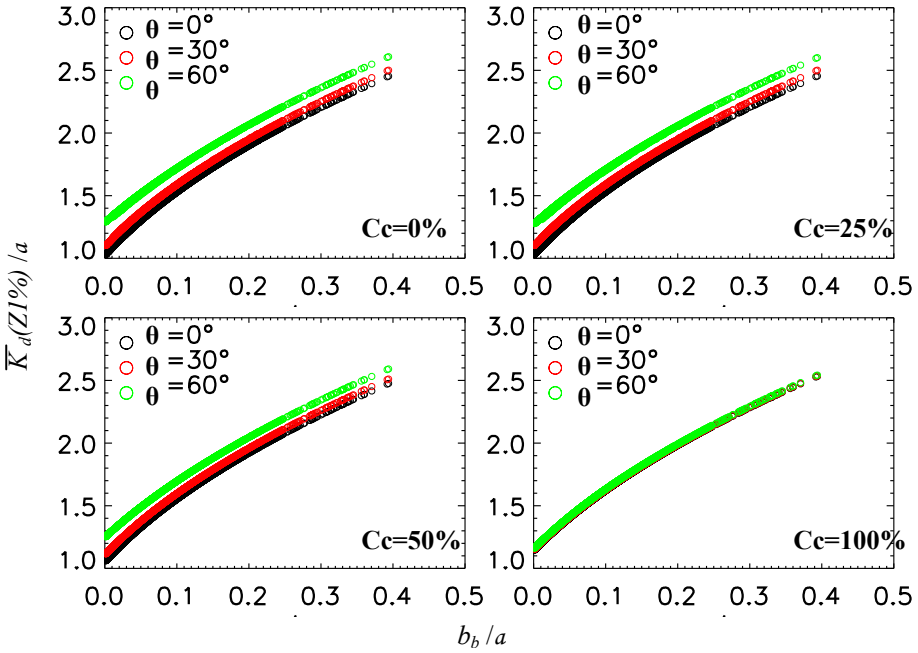


Figure 3: $\overline{K}_d(Z_{1\%})/a$ versus $b_b/a$ for varying sun zenith angles (0°, 30° and 60°). Each graph shows about 2500 $\overline{K}_d(Z_{1\%})/a$ data corresponding to the 100 pairs of IOPs taken at 31 wavelengths and computed for a given percentage of cloud cover (Cc=0, 25, 50 and 100%).

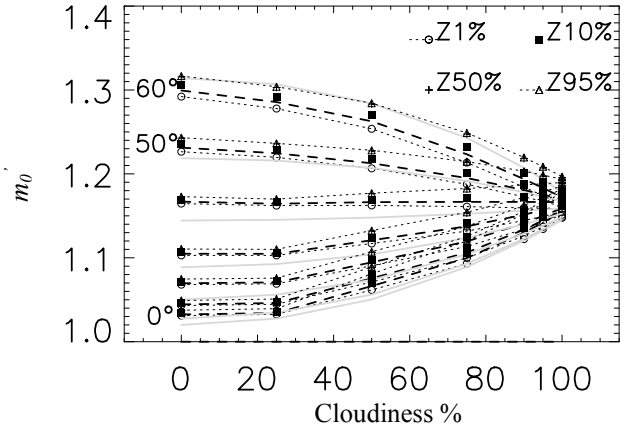


Figure 4: The variations of $m_0'$ with cloudiness and sun zenith angle. $m_0'$ values are derived by non linear regression analysis of Eq(8), using respectively $\overline{K}_d(Z_{1\%})$, $\overline{K}_d(Z_{10\%})$, $\overline{K}_d(Z_{50\%})$ and $\overline{K}_d(Z_{95\%})$ and $b_b/a$ datasets. A different symbol is used for each photic depth as indicated in the figure, the dotted black lines show $m_0'$ for $\overline{K}_d(Z_{1\%})$ and $\overline{K}_d(Z_{95\%})$. The bold black dashed line is the average value of $m_0'$ over the 4 photic depths and the grey line is the model of Eq(13).

A look-up-table for $m_0^{'}$ is constructed from the average values computed above, for each sun zenith angle, $\theta$ and cloud cover, $Cc$. A simpler alternative, giving less accurate results but an easier intuitive interpretation, is to model $m_0^{'}$ in terms of $\theta$ and $Cc$ (or a value of the downwelling average cosine at the surface, $\mu_d^{0+}$, which may give optimal accuracy for ecosystem model studies). Here we propose the approximation for $m_0^{'}$:

$$m_0^{'} = 1.09 + 0.49\cosh(\theta)\cosh(0.7\,Cc) - 0.56\cosh(\theta\,Cc) \quad (13)$$

In the following, we present both $m_1^{'}$ and $m_2^{'}$ coefficients at this photic depth. Future development is needed to include parameterization of the photic depth in such equations.

### 4.2 The variations of $m_1^{'}$

The coefficient $m_1^{'}$ exhibits some similarities with $m_0^{'}$, likely due to the fact that these coefficients are the depth-integrated values of the inverse average cosine ($1/\mu_d$), and of the factor $r_d/\mu_d$ at local depths respectively. The main difference between $m_0^{'}$ and $m_1^{'}$ is the significantly higher variations of $m_1^{'}$ with the different photic depths (a factor of 1.5 approximately between $m_1^{'}$ for $Z_{1\%}$ and for $Z_{50\%}$), which is attributable to the downwelling shape factor. Note also that $m_1^{'}$ is respectively about 2, 3, 4 and 5 times higher than $m_0^{'}$ for the photic depths $Z_{95\%}$, $Z_{50\%}$, $Z_{10\%}$ and $Z_{1\%}$. Figure 5 shows that $m_1^{'}/m_0^{'2}$ recalls the shape of $m_0^{'}$ (Figure 4), but with inverse effects of the sun zenith angle. The following equation is then proposed for $m_1^{'}/m_0^{'2}$ and is plotted in Figure 5 (grey curves):

$$m_1^{'}/m_0^{'2} = 4.266 - 4.56\cosh(\theta)\cosh(0.73\,Cc) + 5.51\cosh(\theta\,Cc) \quad (14)$$

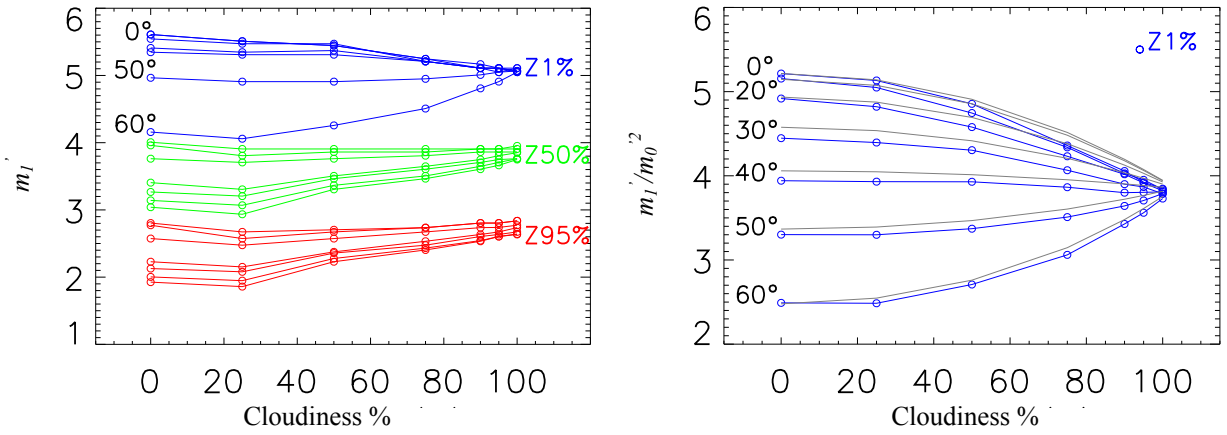


Figure 5: The variations of $m_1^{'}$ (left) with cloudiness and sun zenith angle, for $Z_{1\%}$, $Z_{50\%}$ and $Z_{95\%}$ and of $m_1^{'}/m_0^{'2}$ (right) for $Z_{1\%}$, the grey line (right) displays the modeled $m_1^{'}/m_0^{'2}$ using Eqs (13) and (14).

### 4.3 The variations of $m_2^{'}$

The coefficient $m_2^{'}$ has much higher variability especially between each photic depth (not shown here). It ranges from 0.7 to 6.2 for the full dataset. However, examination of its relation with the coefficient $m_1^{'}$ revealed that it is quite similar to $m_1^{'}$ at almost all sun zenith angles. The ratio $m_2^{'}/m_1^{'}$ is plotted in Figure 6 and shows that it varies slightly for $\theta$<60°. The approximation $m_2^{'} = m_1^{'}$ is then adopted in the model of $\overline{K}_d(Z_{1\%})$.

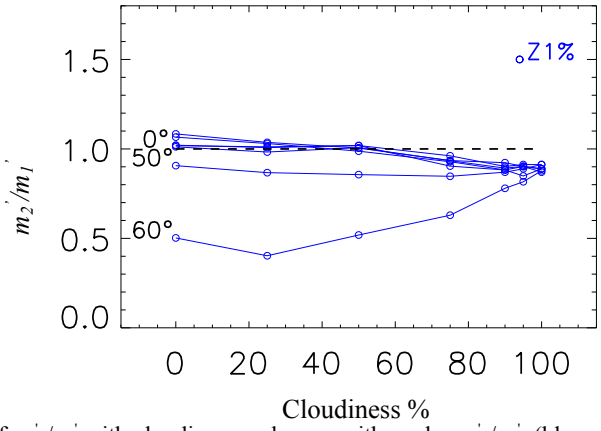


Figure 6: The variations of $m_2'/m_1'$ with cloudiness and sun zenith angle. $m_2'/m_1'$ (blue circles and lines) are derived by non linear regression analysis of equation (8), using $\overline{K}_d(Z_{1\%})$ and $b_b/a$ datasets for the considered values of sun zenith angle and cloudiness. The black dashed line is the approximation for $m_2'/m_1'$.

Validation of this model is carried out by computing the relative error between $\overline{K}_d(Z_{1\%})$ derived from Hydrolight and the modeled $\overline{K}_d(Z_{1\%})$ using Eq(8) where $m_0'$ and $m_1'$ are given respectively by Eqs (13), (14) and assuming $m_2' = m_1'$.The average relative errors found with respect to the full RTE simulation, are less than 1% with maximum errors of 5%, except for the case of θ=60° where relative errors are higher (average relative errors less than 1.7% and 12% for the maximum). This is attributed to the approximation made on $m_2'$, and proves that this term becomes important for higher sun zenith angles. Figure 7 shows the scatterplot of the modeled and Hydrolight-derived $\overline{K}_d(Z_{1\%})$.

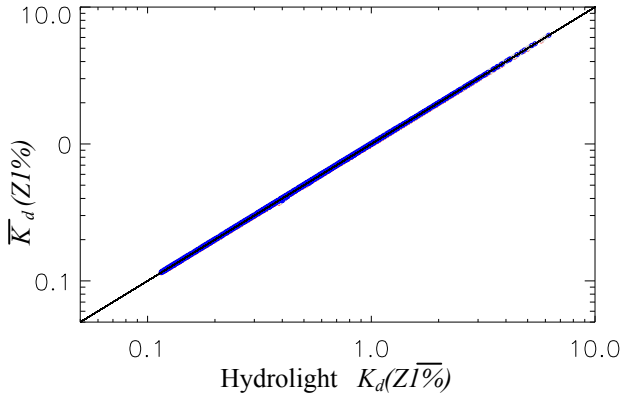


Figure 7**:** The modeled $\overline{K}_d(Z_{1\%})$ versus Hydrolight $\overline{K}_d(Z_{1\%})$ for all the pairs of $a$ and $b_b$, at each wavelength, sun zenith angles, cloudiness values listed in Table 2 (about 49 times 2500 data).

## 5. KPAR

$PAR$ values were computed from the downwelling irradiance fields, $E_d(\lambda)$ provided by Hydrolight, by their spectral integration over the range [400nm-700nm], using Eq(1) for $E_d(\lambda)$ instead of the scalar irradiances $E_o(\lambda)$. The photic depths for $PAR$, noted hereafter $ZPAR_{x\%}$ ($x$=1,10,50,95), were derived from the $PAR$ profiles in a similar way as described previously for the photic depths $Z_{x\%}$ in section 3, 67 $ZPAR_{1\%}$ were obtained from the total set of 100 pairs, for

each sun zenith angle and cloudiness value. $\overline{K}_d PAR$ were then estimated for each photic depth $ZPAR_{x\%}$ as: $\overline{K}_d PAR\left(ZPAR_{x\%}\right) = -\log\left(x\%\right) / ZPAR_{x\%}$ .

High correlation coefficients (>98%) were found between $\overline{K}_d PAR$ and $K_d$ at 590nm for the euphotic depths $Z_{1\%}$ and $Z_{10\%}$, and at 510nm for $Z_{50\%}$. Figure 8 shows a plot of $\overline{K}_d PAR$ versus $\overline{K}_d\left(Z1\%\right)$ at 590nm, for the set of 7x7x67 pairs of ($a$, $b_b$) (times the cloudiness and sun zenith angle values). A non linear relationship was established based on this dataset, and led to the following equation:

$$\overline{K}_d PAR^{\mathrm{mod}}_{ZPAR1\%} = 2.1 \log\left(1 + \overline{K}^{590nm}_{dZ1\%}\right) - 0.23 \qquad (15)$$

This relationship was applied to $\overline{K}^{590nm}_{dZ1\%}$ derived from HYDROPLIGHT, which provided the estimates of $\overline{K}_d PAR_{Z1\%}$ with a relative error (with respect to the $\overline{K}_d PAR$ from the full RTE) less than 5%. Comparison between the Hydrolight $\overline{K}_d PAR_{Z1\%}$ and $\overline{K}_d PAR^{\mathrm{mod}}_{Z1\%}$ shows that relative errors are less than 7% with a maximum of 25%, except for higher sun zenith angle θ=60° where the maximum relative error reaches 40% and the average error ranges from 6% to 9%.

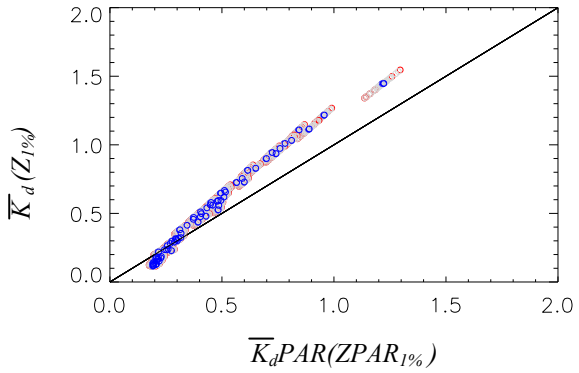


Figure 8: $\overline{K}_d\left(Z_{1\%}\right)$ [m$^{-1}$] at 590nm versus $\overline{K}_d PAR\left(ZPAR_{1\%}\right)$ [m$^{-1}$]. Linear regression analysis of these data gives the blue line and the non linear regression analysis provides the green line. The relationships are derived from 67 data where $ZPAR_{1\%}$ and $Z_{1\%}$ could be computed for the 100 pairs of (a,b), shown as red circles for Cc=0%, blue for Cc=100% and grey for Cc=25 to 95%.

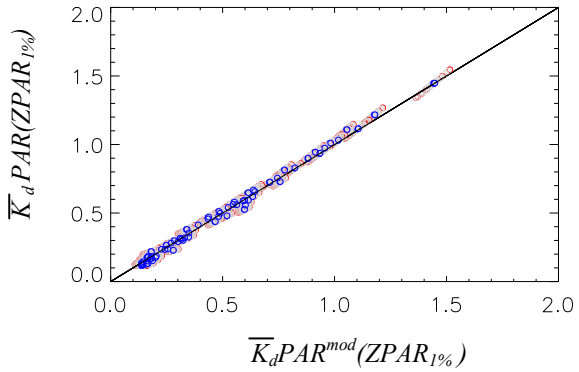


Figure 9: $\overline{K}_d PAR\left(ZPAR_{1\%}\right)$ from HYDROLIGHT versus $\overline{K}_d PAR^{\mathrm{mod}}\left(ZPAR_{1\%}\right)$ modeled from $\overline{K}_d\left(Z_{1\%}\right)$ using Eq(15), plotted for the 7 values of sun zenith angle and 7 percentage cloudiness listed in Table 2. The colour code is the same as in Figure 7.

## 6. DISCUSSION

For a given $\theta$ (respectively $Cc$) the photic depth mean inverse cosine $m_0^{'}$ may change by 5% (respectively 11%) due to a change in cloudiness (respectively in $\theta$). If we consider a medium with very low backscattering arising from particles, then the absorption and the variations of $m_0^{'}$ with $\theta$ and $Cc$ will be the main factors affecting the light attenuation in water (i.e in very absorbing water $a = 1 m^{-1}$, $\overline{K}_d\left(Z_{1\%}\right)$ vary by 11% in a clear sky and only by 1% in an overcast sky, for all sun zenith angles).

The coefficient $m_0^{'}$ is about 3.2 (respectively 5.3) times lower than $m_1^{'}$ and $m_2^{'}$ for $Z_{1\%}$ at $\theta$=0° (respectively at $\theta$=60°), but the variations of the parameters $m_1^{'}$ and $m_2^{'}$ with $\theta$ and $Cc$ were found to be closely related to those of the photic depth mean inverse cosine, $m_0^{'}$. However, while $m_0^{'}$ varies only slightly with the photic depth, $m_1^{'}$ and $m_2^{'}$ do considerably vary and have different responses following the sun zenith angle (Figures 4, 5 and 6). In this context, $m_0^{'}$, $m_1^{'}$ and $m_2^{'}$ may be described as follows:

- $m_0^{'}$: governs the angular structure of light. This parameter is mainly determined by the direct part of the downwelling irradiance incident onto the water surface and depends weakly on the photic depths. When the ratio of the direct to diffuse irradiance $E_d^{dir} / E_d^{dif}$ becomes negligible, $m_0^{'}$ is no more sensitive to changes in $\theta$. This happens in cloudy sky conditions and in water layers deeper than $Z_{95\%}$ (provided the first water layers below the surface where $E_d\left(z\right) > E_d\left(Z_{95\%}\right)$ are avoided).

- $m_1^{'}$: gives the total amount of the downwelling irradiance that is backscattered over the photic depth, it may be approximated by $m_1^{'}\left(Z_{x\%}\right) \approx m_0^{'}\left(Z_{x\%}\right) \int_0^{Z_{x\%}} r_d\left(z\right) dz / Z_{x\%}$ (since $m_0^{'}$ does not vary significantly with photic depths). Since $m_1^{'}$ increases with photic depths (Figure 5), it indicates that $\int_0^{Z_{x\%}} r_d\left(z\right) dz / Z_{x\%}$ is a function increasing with $Z_{x\%}$. The variations of $m_1^{'}$ mainly report that the diffuse fraction of downwelling light that is backscattered is higher at lower sun zenith angles.

- $m_2^{'}$: is quite similar to $m_1^{'}$ except that it contains the estimation of the diffuse part of the upwelling irradiance backscattered downward. The principal difference between $m_1^{'}$ and $m_2^{'}$ arises at higher sun zenith angles ($\theta \geq 60°$) where $m_2^{'}$ decreases by 50%, which tends to increase $\overline{K}_d\left(Z_{1\%}\right)$.

For the three parameters, the special values obtained at $\theta = 40°$ coincide approximately with the values for a fully clouded sky, say for a completely diffuse light pattern. At this angle, changing the ratio $E_d^{dir} / E_d^{dif}$ has no effect on the underwater light attenuation.

The transition to $\overline{K}_d PAR\left(ZPAR_{1\%}\right)$ was performed via a simple regression analysis to relate $\overline{K}_d PAR\left(ZPAR_{1\%}\right)$ to $\overline{K}_d\left(Z_{1\%}\right)$ at a selected wavelength, where the highest correlation is obtained. It was shown that $\overline{K}_d PAR\left(ZPAR_{1\%}\right)$ may be estimated with an average relative error (with respect to a full RTE computed $\overline{K}_d PAR$) around 7% and maximum errors about 25% for $\theta < 60°$.

A similar method can be applied to retrieve $\overline{K}_d PUR\left(ZPUR_{1\%}\right)$, the diffuse attenuation of the photosynthetically usable radiation:

$$PUR = \int_{400nm}^{700nm} a_{\phi n}^{*}\left(\lambda\right) E_d\left(\lambda\right) d\lambda \ \ [Wm^{-2}] \qquad (16)$$

where $a^*_{\phi n}(\lambda)$ is the specific phytoplankton absorption coefficient, normalized by the maximum specific absorption value found at a wavelength $\lambda_m$ : $a^*_{\phi n}(\lambda) = a^*_{\phi}(\lambda) / a^*_{\phi}(\lambda_m)$. Adopting the specific phytoplankton absorption provided by Lee et al [41] in the IOCCG data set, a relationship was derived between $\overline{K}_d PUR(ZPUR_{1\%})$ and $\overline{K}_d(Z_{1\%})$ at 530nm, where the highest correlation coefficient was obtained:

$$K_d PUR_{ZPUR1\%} = 2.13 \log\left(1.41 + K_{dZ1\%}^{530nm}\right) - 0.75 \quad (17)$$

This shift from 590nm for $\overline{K}_d PAR(ZPAR_{1\%})$ estimation to 530nm for $\overline{K}_d PUR(ZPUR_{1\%})$ is stressed for the photic depth $Z_{10\%}$ where $\overline{K}_d PAR(ZPAR_{10\%})$ is better estimated from $\overline{K}_d(Z_{1\%})$ at 600nm and $\overline{K}_d PUR(ZPUR_{10\%})$ from $\overline{K}_d(Z_{1\%})$ at 500nm. This is explained by the phytoplankton absorption which is maximal in the blue part of the spectrum.

## 7. CONCLUSIONS

Linking $K_d$ to IOPs rather than to the concentrations of water components presents the advantage for such algorithms to be portable to all waters with similar ranges of IOPs, and alleviate the attempt to determine the individual contribution of components to light attenuation, depending on their composition, size, index of refraction…etc. In this study, a model giving $\overline{K}_d(Z_{1\%})$ in terms of absorption $a$ and backscattering $b_b$ was established, extending the model of [34] which parameterizes the effect of the sun zenith angle on light attenuation, to turbid waters and to varying cloudiness. The variations of the parameterized photic depth mean cosine, $m_0^{'}$, and the photic depth diffuse backscatter for downwelling light $m_1^{'}$ and for upwelling light $m_2^{'}$ were addressed and quantified for the euphotic depth $Z_{1\%}$ in terms of $\theta$ and $Cc$. However, this model of $\overline{K}_d(Z_{1\%})$ may be improved by the use of a more realistic representation of the ratio $E_d^{dir} / E_d^{dif}$, through the downwelling average cosine at the water surface, $\mu_d^{0+}$, instead of the cloud fraction, $Cc$.

$\overline{K}_d PAR(ZPAR_{1\%})$ was derived from $\overline{K}_d(Z_{1\%})$ and enables the estimation of *PAR* at $Z_{1\%}$ from *PAR(0)* at water surface. Since $\overline{K}_d PAR$ (and $\overline{K}_d PUR$) is depth dependent [42], a parameterization of $\overline{K}_d PAR$ (and $\overline{K}_d PUR$) for varying photic depths $Z_{x\%}$ ($x$ =1, …, 99) could be carried out to provide ecosystem models with more precise estimations of *PAR* along the water column.


## ACKNOWLEDGEMENTS

This study is supported by the Belcolour-2 project funded by the STEREO programme of the Belgian Science Policy Office (under contract SR/00/104). John Cullen is acknowledged for drawing our attention to the growing interest on modeling PUR for ecosystem models. Zhongping Lee and Frederic Mélin are thanked for their comments regarding the parameterization of cloudiness in radiative transfer models.


## REFERENCES


[1] S. W. Nixon, "Coastal marine eutrophication: a definition, social causes, and future concerns", Ophelia, 41 199-219, (1995).

[2] J. E. Cloern, "The relative importance of light and nutrient limitation of phytoplankton growth: a simple index of coastal ecosystem sensitivity to nutrient enrichment", Aquatic Ecology, 33 3-16, (1999).

[3] O. Le Pape, Y. Del Amo, A. Ménesguen, A. Aminot, B. Quequiner, and P. Treguer, "Resistance of a coastal ecosystem to increasing eutrophic conditions: the Bay of Brest (France), a semi-enclosed zone of Western Europe ", Continental Shelf Research, 16 1885-1907, (1996).

[4] A. W. Visser and L. Kamp-Nielsen, "The use of Models in Eutrophication Studies", vol. 52. Washington D. C.: American Geophysical Union, (1996).

[5] A. B. Branco and J. N. Kremer, "The relative importance of chlorophyll and colored dissolved organic matter (CDOM) to the prediction of the diffuse attenuation coefficient in shallow estuaries", Estuaries, 28 (5), 643-652, (2005).

[6] D. Christian and Y. P. Sheng, "Relative influence of various water quality parameters on light attenuation in Indian River Lagoon", Estuarine, Coastal and Shelf Science, 57 961-971, (2003).

[7] M. Huret, F. Gohin, D. Delmas, C. Lunven, and V. Garçon, "Use of SeaWiFS data for light availability and parameter estimation of a phytoplankton production model of the Bay of Biscay", Journal of Marine Systems, 65 (1-4), 509-531, (2007).

[8] M. J. Devlin, J. Barry, D. K. Mills, R. J. Gowen, J. Foden, D. Sivyer, and P. Tett, "Relationships between suspended particulate material, light attenuation and Secchi depth in UK marine waters", Estuarine, Coastal and Shelf Science, 79 429-439, (2008).

[9] G. Lacroix, K. Ruddick, Y. Park, N. Gypens, and C. Lancelot, "Validation of the 3D biogeochemical model MIRO&CO with field nutrient and phytoplankton data and MERIS-derived surface chlorophyll *a* images", Journal of Marine Systems, 64(1-4) 66-88, (2007).

[10] M. Huret, I. Dadou, F. Dumas, P. Lazure, and V. Garçon, "Coupling physical and biogeochemical processes in the Rı´o de la Plata plume", Continental Shelf Research, 25 629-653, (2005).

[11] T. Tian, A. Merico, J. Su, J. Staneva, K. H. Wiltshire, and K. Wirtz, "Importance of resuspended sediment dynamics for the phytoplankton spring bloom in a coastal marine ecosystem", Journal of Sea Research, 62 (4), 214-228, (2009).

[12] E. Sakshaug, A. Bricaud, Y. Dandonneau, P. G. Falkowski, D. A. Kiefer, L. Legendre, A. Morel, J. Parslow, and M. Takahashi, "Parameters of photosynthesis: definitions, theory and interpretation of results", Journal of Plankton Research, 19 (11), 1637-1670, (1997).

[13] S. Markager and W. E. Vincent, "Light absorption by phytoplankton: development of a matching parameter for algal photosynthesis under different spectral regimes", Journal of Plankton Research, 23 (12), 1373-1384, (2001).

[14] H. R. Gordon and D. K. Clark, "Remote sensing optical properties of a stratified ocean: an improved interpretation", Applied Optics, 19 3428-3430, (1980).

[15] R. W. Austin and T. J. Petzold, "The determination of the diffuse attenuation coefficient of sea water using the Coastal Zone Color Scanner (CZCS)", in Oceanography from Space, J. F. R. Gower, Ed. New York: Plenum Press, pp. 239-255. (1981).

[16] R. W. Gould and R. A. Arnone, "Extending Coastal Zone Color Scanner estimates of the diffuse attenuation coefficient into Case II waters", in Ocean Optics XII, vol. 2258, J. S. Jaffe, Ed.: Proc. SPIE, pp. 342-356. (1994).

[17] J. L. Mueller and C. C. Trees, "revised SeaWiFS prelaunch algorithm for diffuse attenuation coefficient K(490)", (1997).

[18] H. Loisel, D. Stramski, B. G. Mitchell, F. Fell, V. Fournier-Sicre, B. Lemasle, and M. Babin, "Comparison of the ocean inherent optical properties obtained from measurements and inverse modeling", Applied Optics, 40 2384-2397, (2001).

[19] Z. Lee, M. Darecki, K. L. Carder, C. O. Davis, D. Stramski, and W. J. Rhea, "Diffuse attenuation coefficient of downwelling irradiance: an evaluation of remote sensing methods", Journal of Geophysical Research, 110 (C02107), (2005).

[20] A. Morel, "Optical modelling of the upper ocean in relation to its biogenous matter content (Case I waters)", Journal of Geophysical Research, 93 10749-10768, (1988).

[21] A. Morel, D. Antoine, and B. Gentili, "Natural variability of bio-optical properties in Case 1 waters: attenuation and reflectance within the visible and near-UV spectral domains, as observed in South Pacific and Mediterranean waters", Biogeosciences, 4 913-925, (2007).

[22] R. C. Smith and K. S. Baker, "Optical classification of natural waters", Limnology and Oceanography, 32 (2), 260-267, (1978).

[23] F. Gohin, S. Loyer, C. Lunven, C. Labry, J.-M. Froidefond, D. Delmas, M. Huret, and A. Herbland, "Satellite-derived parameters for biological modelling in coastal waters: illustration over the eastern continental shelf of the Bay of Biscay", Remote Sensing of Environment, 95 (1), 29-46, (2005).

[24] H. R. Gordon, "Can the Lambert-Beer Law Be Applied to the Diffuse Attenuation Coefficient of Ocean Water?" Limnology and Oceanography, 34 1389-1409, (1989).

[25] J. T. O. Kirk, "Light and Photosynthesis in Aquatic Ecosystems", Second edition ed. UK: Cambridge University Press, (1994).

[26] H. R. Gordon, O. B. Brown, and M. M. Jacobs, "Computed relationships between inherent and apparent optical properties of a flat, homogeneous ocean", Applied Optics, 14 417-427, (1975).

[27] J. T. O. Kirk, "Monte Carlo study of the underwater light field in, and relationships between optical properties of, turbid yellow waters", Australian Journal of Freshwater Research, 32 517-532, (1981).

[28] C. D. Mobley, "Light and water: radiative transfer in natural waters". London: Academic Press, (1994).

[29] R. H. Stavn and A. D. Weidemann, "Shape factors, two-flow models, and the problem of irradiance inversion in estimating optical parameters", Limnology and Oceanography, 34 (8), 1426-1441, (1989).

[30] A. G. Dekker, V. E. Brando, J. M. Anstee, N. Pinnel, T. Kutser, E. J. Hoogenboom, S. Peters, R. Pasterkamp, R. Vos, C. Olbert, and T. J. M. Malthus, "Imaging Spectrometry of Water", in Imaging Spectrometry, F. D. Van der Meer and S. M. de Jong, Eds. Netherlands: Kluwer, pp. 307-359. (2001).

[31] E. Aas, "Two-stream irradiance model for deep waters", Applied Optics, 26 2095-2101, (1987).

[32] S. Sathyendranath, T. Platt, C. M. Caverhill, R. E. Warnock, and M. R. Lewis, "Remote sensing of oceanic primary production: Computations using a spectral model", Deep Sea Res., 36 (3A), 431-453, (1989).

[33] J. T. O. Kirk, "Volume scattering function, average cosines, and the underwater light field", Limnol. Oceanogr, 36 (3), 455-467, (1991).

[34] Z. Lee, K. Du, and R. Arnone, "A model for the diffuse attenuation coefficient of downwelling irradiance", Journal of Geophysical Research, 110 (C02016), (2005).

[35] H. R. Gordon, O. B. Brown, R. H. Evans, J. W. Brown, R. C. Smith, K. S. Baker, and D. K. Clark, "A semianalytical radiance model of ocean color", Journal of Geophysical Research, 93 (D9), 10909-10924, (1988).

[36] W. W. Gregg and K. L. Carder, "A simple spectral solar irradiance model for cloudless maritime atmospheres", Limnology and Oceanography, 35 (8), 1657-1675, (1990).

[37] F. Kasten and G. Czeplak, "Solar and terrestrial radiation dependent on the amount and type of clouds", Solar Energy, 24 177-189, (1980).

[38] IOCCG, "Remote Sensing of Inherent Optical Properties: Fundamentals, Tests of Algorithms, and Applications." (2006).

[39] R. C. Smith and K. S. Baker, "Optical properties of the clearest natural waters (200-800nm)", Applied Optics, 20 177-184, (1981).

[40] J. T. O. Kirk, "Dependence of the relationship between inherent and apparent optical properties of water on solar attitude", Limnology and Oceanography, 35 1486-1582, (1984).

[41] Z.-P. Lee, K. L. Carder, and R. Arnone, "Deriving inherent optical properties from water color: a multi-band quasi-analytical algorithm for optically deep waters", Applied Optics, 41 5755-5772, (2002).

[42] Z. Lee, "KPAR: an optical property associated with ambigous values", Journal of Lake Sciences, 21 (2), 159-164, (2009).